Proceedings of Czech–Japanese Seminar in Applied Mathematics 2004
August 4-7, 2004, Czech Technical University in Prague
http://geraldine.fjfi.cvut.cz
pp. 63–72

FLOW OVER A GIVEN PROFILE IN A CHANNEL WITH DYNAMICAL EFFECTS

JIŘÍ FÜRST[1] , RADEK HONZÁTKO[2] , JAROMÍR HORÁČEK[3] , AND KAREL KOZEL[1]

Abstract. The work deals with a numerical solution of steady and unsteady 2D inviscid incompressible flow over the profile NACA 0012 in a channel. The flow is described by the system of Euler equations. Cell-centered finite-volume scheme at quadrilateral C-mesh is used. Steady state solutions and also unsteady flows caused by the prescribed oscillation of the profile were computed. The method of artificial compressibility and the time dependent method are used for computation of the steady state solution. Some presented numerical results are compared with experimental data.

Key words. aeroelasticity, cell-centered scheme, Euler equations, finite-volume method, method of artificial compressibility, oscillation, time dependent method

AMS subject classifications. 74F10, 76B10

1. Introduction. The cell-centered Lax-Wendroff scheme in Richtmyer form of second order accuracy is considered for the numerical solution of flow over the profile NACA 0012 in a channel. The added artificial viscosity is used in the combination with the Lax-Wendroff scheme.

2. Mathematical model. The behaviour of a flow is described by the system of Euler equations for inviscid incompressible flow in conservation form:

$$\tilde{R}W_t + F_x + G_y = 0 \ , \tag{2.1}$$

where

$$W = \begin{pmatrix} \frac{p}{\rho} \\ u \\ v \end{pmatrix}, \ F = \begin{pmatrix} u \\ u^2 + \frac{p}{\rho} \\ uv \end{pmatrix}, \ G = \begin{pmatrix} v \\ uv \\ v^2 + \frac{p}{\rho} \end{pmatrix}, \ \tilde{R} = \operatorname{diag} \|0, 1, 1\| \, .$$

The system written above is used for the numerical solution with $\tilde{R} = \operatorname{diag} \left\| \frac{1}{a^2}, 1, 1 \right\|$, $a \in R$ (method of artificial compressibility).

Here ρ is the density (constant), p is the pressure and (u, v) is the velocity vector.

Upstream conditions are $u = u_\infty$, $v = v_\infty$, p is extrapolated. Downstream condition is only given by $p = p_2$. Next values of W_2 are extrapolated. Wall conditions on fixed walls of the channel are non-permeability conditions $(u, v)_n = 0$ (normal component of velocity vector is equal to zero). Two approaches were applied to the wall conditions on the oscillating profile in the channel. Firstly the non-permeability conditions were applied, secondly the velocity vector of the flow field near the profile

[1]Department of Technical Mathematics, Faculty of Mechanical Engineering, Czech Technical University in Prague, Karlovo nám. 13, 120 00 Prague, Czech Republic.
[2]Department of Mathematics, Faculty of Nuclear Sciences and Physical Engineering, Czech Technical University in Prague, Trojanova 13, 120 00 Prague, Czech Republic.
[3]Institute of Thermomechanics, Academy of Sciences of the Czech Republic, Dolejškova 5, 182 00 Prague, Czech Republic.

boundary is determined by the velocity vector normal to the profile boundary and given by the angular velocity of the profile.

The method of artificial compressibility (MAC) and the time dependent method (TDM) are used for the computation of the steady state solution. The MAC represents one possibility how to solve the boundary-value problem (BVP) for the system (2.1). The method lies in the substitution of the BVP by an initial-boundary-value problem (IBVP) for the system

$$MW_t + F_x + G_y = 0 \ ,$$

where M is an optional regular matrix (in our case $M = \mathrm{diag}\|\frac{1}{a^2}, 1, 1\|$). If boundary conditions for IBVP are stationary and identical to them for the original BVP, the steady solution of the IBVP (if it exists) will also satisfy the original BVP. The introduction of time derivative of pressure gives us the continuity equation of suppositional incompressible fluid satisfying equation of state for ideal gas. The TDM represents the fusing of the IBVP solution in artificial time. The advantage of joint of the MAC and TDM is possibility for using well-known methods for solution of compressible fluid flow, see, e. g. Chorin [11].

In the case of unsteady solution it is supposed $a \to \infty$ or $a \gg K$, where K is a given (big) positive number.

2.1. Prescribed oscillation of the profile. The change of attack angle of the profile fixed in the point of elastic axis is given by the formula

$$\varphi = \varphi_0 \sin(2\pi f t) \ , \tag{2.2}$$

where φ $[rad]$ is the angle of rotation of the profile from the equilibrium position, φ_0 is the amplitude of oscillations, f $[s^{-1}]$ is the frequency and t $[s]$ is time.

3. Numerical solution.

3.1. Numerical scheme - Lax-Wendroff. The Lax-Wendroff (Richtmyer form) scheme in a form of predictor-corrector with added artificial viscosity is used at quadrilateral C-mesh (m=4) in a cell-centered form:

- LW Richtmyer predictor:

$$W_i^{n+1/2} = W_i^n - \frac{1}{2}\frac{\Delta t}{\mu_i}\sum_{k=1}^{m}(\bar{F}_{ik}^n \Delta y_k - \bar{G}_{ik}^n \Delta x_k) + \frac{\varepsilon}{m}\sum_{k=1}^{m}(W_k^n - W_i^n)$$

- LW Richtmyer corrector:

$$\tilde{W}_i^{n+1} = W_i^n - \frac{\Delta t}{\mu_i}\sum_{k=1}^{m}(\bar{F}_{ik}^{n+1/2} \Delta y_k - \bar{G}_{ik}^{n+1/2} \Delta x_k) \ ,$$

$$W_i^{n+1} = \tilde{W}_i^{n+1} + \mathrm{AD}W_i^n,$$

where $\mathrm{AD}W_i^n$ is artificial viscosity

and $\bar{F}_{ik} = \frac{1}{2}(F_i + F_k), \bar{G}_{ik} = \frac{1}{2}(G_i + G_k), \varepsilon \in (0, 1\rangle$.

The artificial viscosity coefficient ε has the constant value in our computations. This value can be changed with respect to convergence speed.

The superscript n represents time level, subscripts i and k represent local cell indexing (see Figure 3.1). Symbol μ_i denotes volume of the current cell indexed by i, F_i, F_k, G_i, G_k are vectors of inviscid fluxes evaluated in centres of cells corresponding to the subscript.

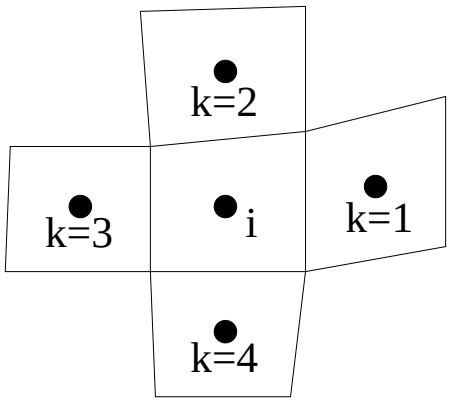

Fig. 3.1. *Local indexing of neighbouring cells.*

3.2. Numerical scheme - AUSM scheme. The AUSM (Advection Upstream Splitting Method) scheme for inviscid low-Mach-number flow is presented. This scheme was used by J. Fürst [8] for the steady state numerical solution of external aerodynamics problem and his numerical data are compared with the data obtained by the above mentioned Lax-Wendroff scheme (see Figures 4.7, 4.8).

The equations for compressible flows are given by

$$\Gamma Q_\tau + F_x + G_y = 0 \ , \tag{3.1}$$

$$Q = \begin{pmatrix} p \\ u \\ v \\ T \end{pmatrix}, \ F = \begin{pmatrix} \rho u \\ \rho u^2 + p \\ \rho uv \\ \rho uH \end{pmatrix}, \ G = \begin{pmatrix} \rho v \\ \rho uv \\ \rho v^2 + p \\ \rho vH \end{pmatrix} \ ,$$

where p is the pressure, (u, v) is the velocity vector, T denotes the temperature, ρ is the density and H is the total enthalpy given by

$$H = \frac{\gamma}{\gamma - 1}\frac{p}{\rho} + \frac{1}{2}(u^2 + v^2) \ .$$

γ denotes the Poisson constant.

The preconditioner Γ is

$$\Gamma = \begin{bmatrix} \Theta & 0 & 0 & \rho_T \\ 0 & \rho & 0 & 0 \\ 0 & 0 & \rho & 0 \\ \Theta H & 0 & 0 & \rho_T H + \rho C_p \end{bmatrix} \ , \tag{3.2}$$

where $\Theta = 1/a^2$, parameter a has the dimension of velocity and the similar meaning as parameter a in the section 2, C_p is the specific heat at constant pressure, ρ_T is the derivative of ρ with respect to T. With this form of the preconditioner a comparison between incompressible flow and low-Mach-number compressible flow can be made directly.

The preconditioner (3.2) is before its simplification equivalent to the preconditioner used by Turkel [10]. It is formulated in variables $Q = (p, u, v, S)^T$, where S is

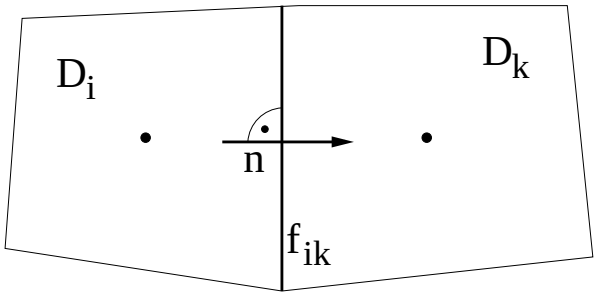

Fig. 3.2. *Symbols concerning the numerical flux (3.3).*

the entropy, $S = \ln \frac{p}{\rho^\gamma}$. The form of the preconditioner is

$$\tilde{\Gamma} = \begin{bmatrix} \frac{c^2}{\omega} & 0 & 0 & \delta \\ \frac{\alpha u}{\rho\omega} & 1 & 0 & 0 \\ \frac{\alpha v}{\rho\omega} & 0 & 1 & 0 \\ 0 & 0 & 0 & 1 \end{bmatrix},$$

δ, α are parameters (see Turkel [10]), c is sound speed, $\omega = K(u^2 + v^2)$, K is a constant (see Turkel [10]).

Numerical flux

$$\tilde{H}\mathbf{n}|_{ik} = (u_{ik}n_x + v_{ik}n_y) \begin{pmatrix} 0 \\ \rho u \\ \rho v \\ 0 \end{pmatrix}_{i|k} + \begin{pmatrix} (\rho u)_{ik}n_x + (\rho v)_{ik}n_y \\ p_{ik}n_x \\ p_{ik}n_y \\ (\rho u H)_{ik}n_x + (\rho v H)_{ik}n_y \end{pmatrix} - F_d \tag{3.3}$$

through a common face f_{ik} of finite volumes D_i and D_k in the normal direction $\mathbf{n} = (n_x, n_y)$ to this face from D_i to D_k (see Figure 3.2) has the convective part discretized with velocity upwinding. The acoustic part can be discretized for instance centrally. The vector $\mathbf{n}$ has the length of the face f_{ik}. The index ik expresses values on the face f_{ik} and the index $i|k$ expresses the upwinding discretization, where the values are taken from D_i if $(u_{ik}n_x + v_{ik}n_y) > 0$ otherwise from D_k. The last term F_d in (3.3) denotes an artificial dissipation term

$$F_d = \begin{pmatrix} \frac{p_k - p_i}{\beta} + (q\rho_T)_{ik}(T_k - T_i) \\ 0 \\ 0 \\ H_{ik}\frac{p_k - p_i}{\beta} \end{pmatrix},$$

where $q = \sqrt{u^2 + v^2}$ and β can be chosen either as a global velocity or as a local velocity q.

More details of the discretization of convective and acoustic part of the numerical flux (3.3) are presented in, e. g., [7].

The backward Euler discretization in time is used.

3.3. Wall conditions. Wall conditions are realized by using of "reflection principle", i. e. there are artificial volumes in the wall created by a reflection on the wall. The velocity vector (u, v) is also reflected on the wall.

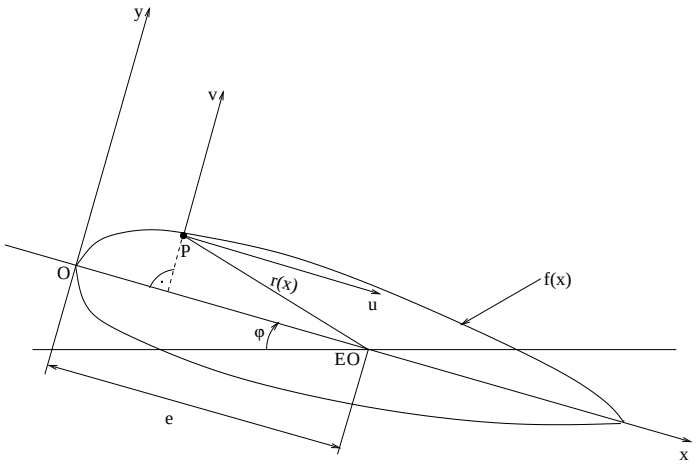

FIG. 3.3. *Meaning of symbols in the equation (3.4).*

Wall conditions on the oscillating profile are realized by using "small disturbance theory" because only small changes of the angle φ are considered. The motion of the profile is approximated by the rotation of the normal vector to the profile boundary ($\frac{\partial(u,v)}{\partial s} = f' + \varphi$, where f is a function describing the profile shape, s is a tangential vector to the profile and $|\varphi| \leq 6^0$). Another method how to treat the oscillating profile is to employ the Arbitrary Lagrangian-Eulerian method, see, e. g., [2].

Two different approaches to a numerical realization of the wall conditions on the oscillating profile were applied. Firstly the non-permeability condition is used in every time, secondly the following condition is used:

$$\left(-\frac{df}{dx}\right) u + v = \dot{\varphi} f(x) \left(-\frac{df}{dx}\right) + \dot{\varphi}(e - x) \ , \tag{3.4}$$

where (u, v) is the velocity vector, $\dot{\varphi}$ is the angular velocity for the profile rotation, $f(x)$ is a function describing the shape of the profile surface and e is the distance of the elastic axis EO from the origin O of a local coordinate system.

All quantities in the equation (3.4) are related to the local coordinate system with the origin O (see Figure 3.3).

3.4. Non-dimensional variables. The non-dimensional variables U, V, P, T are used for the numerical solution. The relations between dimensional and non-dimensional variables are given by the normalization of the dimensional variables u, v, p, ρ, t with reference (dimensional) values u_∞, v_∞, l_{ref} as follows: $X = \frac{x}{l_{\text{ref}}}$, $Y = \frac{y}{l_{\text{ref}}}$, $P = \frac{p}{\rho q_{\text{ref}}^2}, U = \frac{u}{q_{\text{ref}}}$, $V = \frac{v}{q_{\text{ref}}}$, $T = \frac{t q_{\text{ref}}}{l_{\text{ref}}}$, where $q_{\text{ref}} = \sqrt{u_\infty^2 + v_\infty^2}$.

The system (2.1) has in the non-dimensional variables the following form

$$\tilde{R} W_T + F_X + G_Y = 0 \ , \tag{3.5}$$

where $W = (P, U, V)^T$, $F = \left(U, U^2 + P, UV\right)^T$, $G = \left(V, UV, V^2 + P\right)^T$, $\tilde{R} = \text{diag}\,\|0, 1, 1\|$.

The system written above is used for the numerical solution with the diagonal matrix $\tilde{R} = \text{diag}\left\|\frac{q_{\text{ref}}^2}{a^2}, 1, 1\right\|$, $a \in R$.

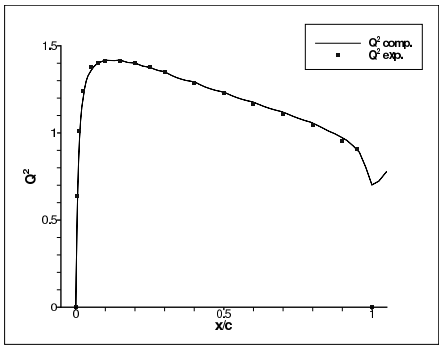

Fig. 4.1. *Comparison of computed and experimental data, distribution of* $Q^2 = U^2 + V^2$ *along the walls of the profile.*

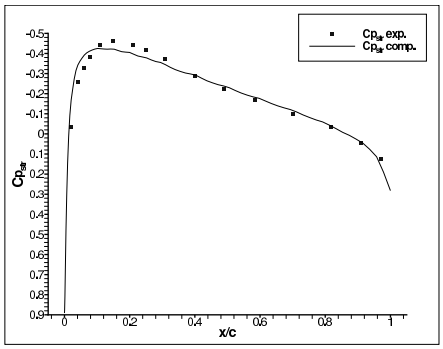

Fig. 4.2. *Comparison of computed and experimental data, distribution of* C_p *coefficient along the walls of the profile.*

4. Numerical results. Numerical results over the profile NACA 0012 in the channel are presented. The quality of the capturing of the blunt leading edge of the profile is very important for the quality of numerical results. The finite volume C-mesh is used. For more details for creating this type of mesh, see, e. g., [1]. Figure 4.9 shows zoomed part of the C-mesh in the close area around the profile used for external aerodynamics computation.

Figures 4.1, 4.2 and 4.3 represent the steady state solution of the flow over the profile NACA 0012 achieved at the C-mesh for the angle of attack equal to $\varphi = 0^o$.

Figure 4.1 compares distribution of squared non-dimensional fluid velocity $Q^2 = U^2 + V^2$ on the walls of the profile for computed and experimental data obtained from [3].

Figure 4.2 presents comparison of C_p coefficient along the walls of the profile for computed and experimental data obtained from [4] and recomputed with respect to incompressible flow by use of Prandtl-Glauert correction. The formula for the C_p coefficient has the following form

$$C_p = \frac{p - p_2}{\frac{1}{2}\rho q_{\text{ref}}^2} \ .$$

Figure 4.3 shows isolines of non-dimensional velocity Q in the close area to the profile NACA 0012 in the channel.

Table 4.1 presents the comparison of computed and experimental data for the lift C_y. The steady state solutions for different angles of attack φ [degrees] were computed. The experimental data are obtained from [3]. Symbol C_y comp. denotes computed lift and C_y exp. denotes experimental data.

Figures 4.4, 4.5 and 4.6 present the results for the prescribed oscillation of the profile NACA 0012 given by the formula (2.2). The elastic axis is situated in 25% of the profile chord from the local coordinate system origin. The symbol *phi/10* denotes the distribution of the variable φ according to the equation (2.2).

Figure 4.4 shows C_p coefficient during three oscillation periods in points $\frac{x}{c} = 0.2$ on the upper ($C_{p_{up}}$) and lower ($C_{p_{down}}$) wall of the oscillating profile, where c is the length of the profile chord. The frequency of the oscillation is $f = 30$ Hz and the amplitude $\varphi_0 = 3^o$. There are compared results for different values of the coefficient a in this figure - firstly $a = 1$, secondly $a = 10$. The value of the coefficient a is limited through the time step restrictions of explicit finite volume scheme used. The

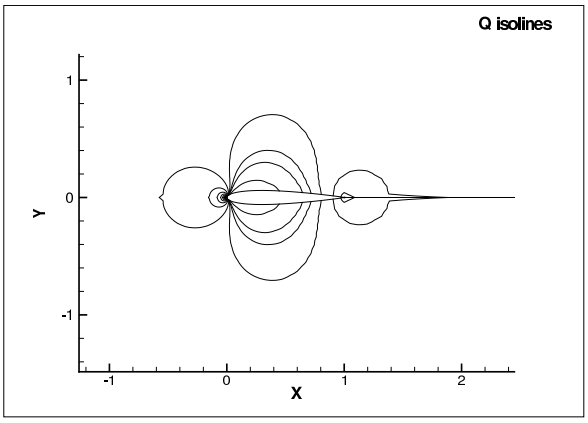

FIG. 4.3. *Isolines of* $Q = \sqrt{U^2 + V^2}$ *in the channel with NACA0012, focused on the area around the profile.*

φ	C_y comp.	C_y exp.
-2	-0.13	-0.15
0	0.00	0.00
2	0.13	0.14
4	0.26	0.30

TABLE 4.1
Comparison of computed and experimental data for lift C_y.

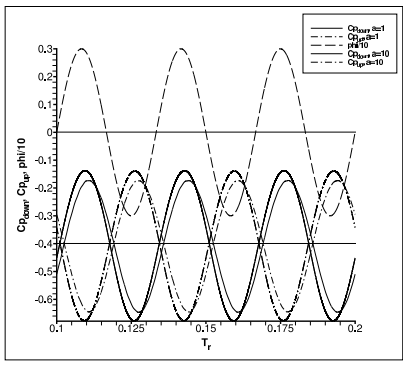

FIG. 4.4. C_p *coefficient in the points* $\frac{x}{c} = 0.2$ *for the oscillating profile with* $f = 30Hz$, *comparison of computed results for* $a = 1$ *and* $a = 10$.

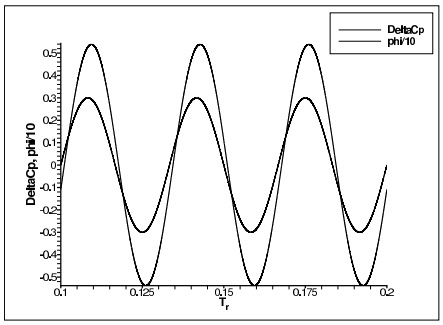

FIG. 4.5. ΔC_p *coefficient for the oscillating profile with* $f = 30Hz$, $a = 10$.

wall conditions are non-permeability conditions. These conditions are not reflecting the influence of the location of the elastic axis of the profile.

Figure 4.5 shows $\Delta C_p = C_{p_{down}} - C_{p_{up}}$ coefficient for the points $\frac{x}{c} = 0.2$. These results are suitable for comparison with available experimental data [4].

Table 4.2 presents the comparison of computed, experimental and theoretical data for oscillating components (real and imaginary part) of ΔC_p for points on the profile boundary with $\frac{x}{c} = 0.2$. The frequency of the oscillation of the profile is $f = 30$Hz and the amplitude is $\varphi_0 = 3^o$. The experimental and theoretical data are the data of Triebstein [9] converted with respect to the amplitude 3 degrees.

Figure 4.6 compares C_p coefficient plotted for points $\frac{x}{c} = 0.2$ on the oscillating profile for the two boundary conditions applied. The boundary conditions (3.4) involve the influence of the position of the elastic axis instead of the simple non-permeability boundary conditions. There is possible to see small differences between the results for these two boundary conditions applied.

	Re ΔC_p	Im ΔC_p
exp. Triebstein	0.494	-0.0325
theo. Triebstein	0.440	-0.114
comp. values	0.529	-0.108

TABLE 4.2

Comparison of computed, experimental and theoretical data for Re ΔC_p and Im ΔC_p.

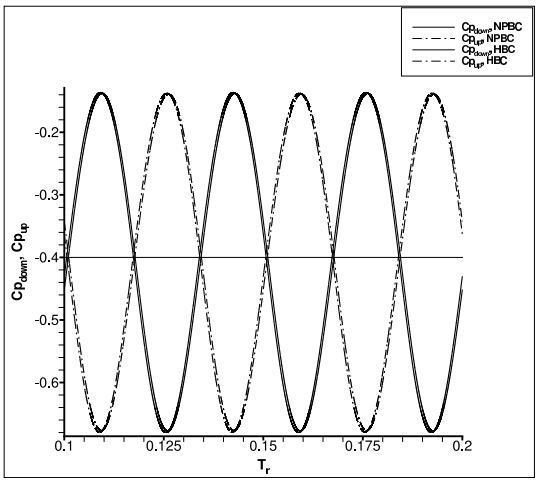

FIG. 4.6. *C_p coefficient in the points $\frac{x}{c} = 0.2$ for the oscillating profile with $f = 30Hz$, comparison of computed results for the two applied boundary conditions.*

Finally, the verification of computed steady state results was done. The distribution of C_p coefficient along the wall of the profile NACA0012 computed by the above mentioned (see 3.1) cell-centered Lax-Wendroff scheme in the case of external aerodynamics was compared with numerical results achieved by modern AUSM scheme (see 3.2) applied to the same problem of external aerodynamics. The comparison is shown in Figure 4.7 from where very good agreement is obvious. The geometry of the computational area is shown in Figure 4.8 and the detail of a close area to the profile in Figure 4.9.

Figure 4.10 compares isolines of C_p coefficient around the profile. The data were computed for the same case of external aerodynamics as mentioned above and shown in Figures 4.8, 4.9.

5. Conclusion. The comparison of computed and experimental data for Q^2 (see Figure 4.1) and C_p coefficient (see Figure 4.2) shows very good agreement.

Table 4.1 also shows quite good agreement of computed and experimental data for the lift C_y.

The comparison of the data in Table 4.2 shows that the computed data for oscillating profile are comparable with those Triebstein's experimental and theoretical data [9].

In the case of the unsteady solution the problem is in the influence of the value of the coefficient a (see matrix $\tilde{R}$ in (2.1)) on the solution. That can be seen in Figure 4.4. Another method how to treat the unsteady solution is the application of the dual time stepping method.

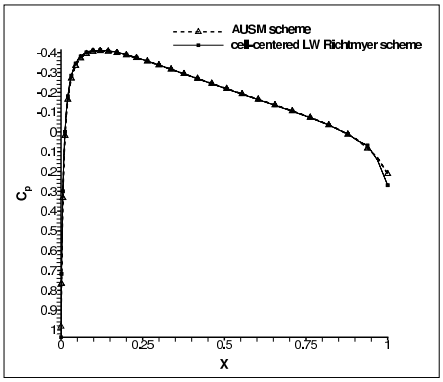

FIG. 4.7. *Distribution of C_p coefficient along the walls of the profile, comparison of computed results achieved by LW Richtmyer and AUSM scheme.*

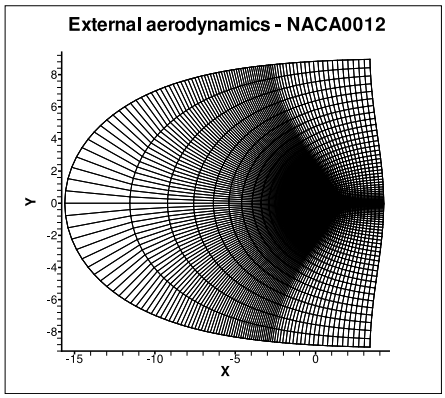

FIG. 4.8. *Computational area - external aerodynamics.*

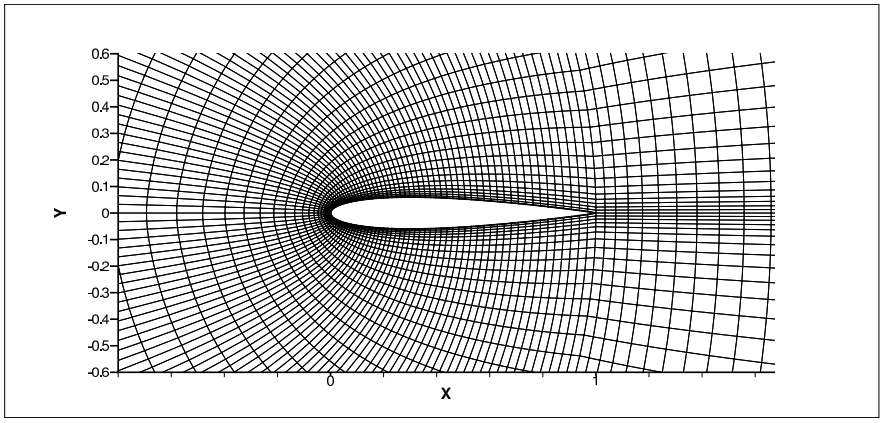

FIG. 4.9. *C-mesh around the profile NACA0012 used for finite-volume method in external aerodynamics, detail near the profile.*

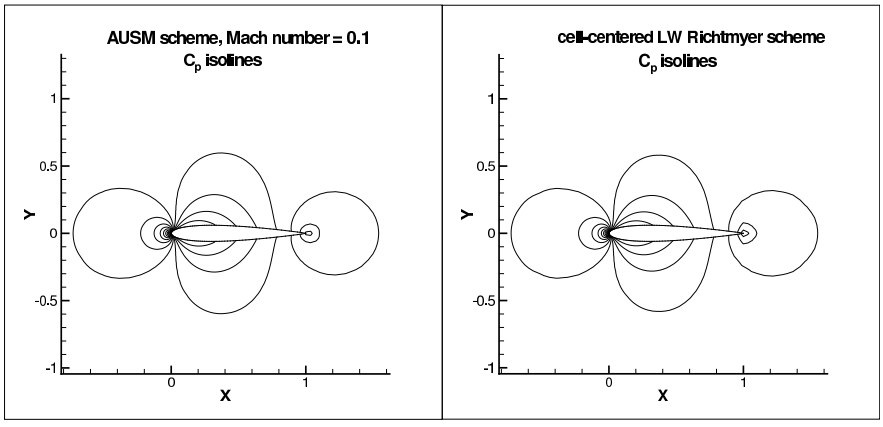

FIG. 4.10. *Isolines of C_p coefficient around the profile.*

It is convenient to compare computed data with different numerical methods. One of them is the finite element method (FEM) applied to the same problem. For details of application of FEM on problems of aeroelasticity, see, e. g., [5].

Acknowledgment. This work was supported by grants No. 201/02/0684 of the Grant Agency of the Czech Republic, Research Plan MSM 210000003, the project "Applied Mathematics in Technology and Physics" MSM 6840770010 of the Ministry of Education of the Czech Republic and 101/02/0391 of the Grant Agency of the Czech Republic.

REFERENCES

[1] A. Shmilovich and D.A. Caughey. Grid generation for wing-tail-fuselage configurations. *Journal of Aircraft*, vol. 22, No. 6 (1985) pp. 467–472.

[2] P. Sváček and M. Feistauer. Application of a Stabilized FEM to Problems of Aeroelasticity. to appear in *Proc. of ENUMATH 2003*, Springer-Verlag, 2004.

[3] J. Luťcha. Proceedings of wing profile characteristics, Report No. 1669/55. (1955) VTA AZ, Brno. (In Czech)

[4] J. Benetka. Experimental data of pressures on oscillating profiles NACA 64A012M5 and NACA 0012. Report of Research and Test Aeronautical Institute, grant No. 101/02/0391, Prague, 2003. (In Czech)

[5] P. Sváček and M. Feistauer and J. Horáček. Numerical Simulation of Flow Induced Airfoil Vibrations. In *Proc. of the 8th International Conference on Flow-Induced Vibration*, FIV2004, pp. 57–62, Paris, 2004.

[6] R. Honzátko, J. Horáček and K. Kozel. Numerical Solution of Steady and Unsteady Flow over Given Profile in a Channel. In *Proceedings Interaction and Feedbacks '2003*, No. 10, pp. 43–50, Institute of Thermomechanics AS CR, Prague, 2003.

[7] J. Vierendeels, K. Riemslagh and E. Dick. A Multigrid Semi-implicit Line-Method for Viscous Incompressible and Low-Mach-Number Flows on High Aspect Ratio Grids. Journal of Computational Physics, No. 154 (1999) pp. 310–341

[8] J. Fürst. Numerical Solution of Compressible Flows Using TVD and ENO Finite Volume Methods. Habilitation, Faculty of Mechanical Engineering, Czech Technical University in Prague, 2004.

[9] H. Triebstein. Steady and Unsteady Transonic Pressure Distributions on NACA0012. Journal of Aircraft, vol. 23, No. 3 (1986) pp. 213–219

[10] E. Turkel. Review of Preconditioning for the Compressible Fluid Dynamic Equations, CFD Review, M. M. Hafez and K. Oshima, editors, John Wiley and Sons, 1998.

[11] A. J. Chorin. A Numerical Method for Solving Incompressible Viscous Flow Problems, Journal of Computational Physics, 2(1), 1967, pp. 12–26.